Journal of Catalysis 257 (2008) 283–290

Contents lists available at ScienceDirect

Journal of Catalysis

www.elsevier.com/locate/jcat

Studies in structural characterization and correlation with the catalytic activity of an efficient and stable WO_x/SBA-15 nanocomposite catalyst

Ankur Bordoloi, S.B. Halligudi *

Inorganic Chemistry and Catalysis Division, National Chemical Laboratory, Pune-411 008, India

ARTICLE INFO

Article history:
Received 6 March 2008
Revised 7 May 2008
Accepted 10 May 2008
Available online 13 June 2008

Keywords:
Tungsten oxide nanocluster
Mesoporous materials
Catalytic oxidation
Sulfides
Sulfoxides

ABSTRACT

A new WO_x/SBA-15 nanocomposite catalyst system was developed by hydrothermal synthesis. The material was characterized by X-ray diffraction, high-resolution transmission electron microscopy, sorption analysis, FT-IR, CP-MAS NMR, XPS, and energy-dispersive X-ray analysis. Various types of aromatic and aliphatic sulfides were selectively oxidized to sulfoxides in good to excellent yields without becoming overoxidized to the sulfones using 70% aq. *tert*-butyl hydrogen peroxide in the presence of nanocomposite catalyst at room temperature. The catalyst could be easily recovered and reused for at least eight reaction cycles under the reaction conditions described here with no significant loss of reactivity.

© 2008 Elsevier Inc. All rights reserved.

1. Introduction

Creation of nanocomposite materials by introducing nanocrystals into a macroscopic matrix is an area of growing interest in catalysis. The functionality of nanocomposites has been attributed to their surface properties, including surface-to-bulk atomic ratio, polyhedral surface morphology, concentrations of surface defects (coordinatively unsaturated ions due to planes, edges, corners, anion/cation vacancies, and electron excess centers), and shape selectivity [1,2]. Immobilization of nanoscopic materials in high-surface area supports with improved catalytic activity and product selectivity is a task of great economic and environmental importance in the chemical and pharmaceutical industries [3]. There are few reports describing the use of mesoporous silica as a support for immobilization tungsten oxide species [4,5]. Zhang et al. described the synthesis of tungsten-containing MCM-41 with good dispersion, but with segregated crystalline WO_x detected after mild thermal treatment [6]. The crystalline phases of WO_x that form at low pH in the presence of H_2O_2 was prevented by the use of oxoperoxometalate precursors. Its stability was poor, as evidenced by the extensive leaching of tungsten species [7]. Recently, atomic layer deposition (ALD) was used to graft tungsten oxide species onto mesoporous silica (SBA-15) [8,9].

The oxygen-transfer reaction is one of the most elementary transformations in synthesis organic chemistry, and several metal-catalyzed oxidation reactions have been investigated to date [10,11]. Among these, oxidation of sulfur compounds to sulfoxides is an interesting and attractive method [12,13]. Sulfoxide is one of the useful building blocks as a chiral auxiliary in organic synthesis [14–18] and plays a key role in enzyme activation [19–22]; however, conventional transformations are only somewhat successful, due to overoxidation and generation of toxic wastes [23–25]. The efficacy of heterogeneous tungstate systems has been dynamically examined, because various tungsten-based homogeneous catalysts are known to exhibit high activity in practical oxidation procedures including epoxidation of alkenes [26,27], oxidation of alcohol [27,28], oxidative cleavage or halogenation of olefins [28], and oxidative desulfurization [29–32]. As a result, some promising heterogeneous systems, such as insoluble polyoxotungstates [33,34], immobilized peroxotungstates, triphasic phosphotungstate [35], and pseudoheterogeneous systems [36], have been reported recently. Inorganic polymers are effective mediators for organizing tungsten oxide species into higher-order composite structures [19–22]. Here we report the synthesis of tungsten oxide and SBA-15 nanocomposite (hereinafter WO_x/SBA-15) with large pore diameters and describe its catalytic activity in the selective oxidation of sulfur compounds to corresponding sulfoxides under ambient reaction conditions.

2. Experimental

2.1. Materials

Sodium tungstate was purchased from Sisco Research Laboratory Pvt. Ltd., India. TEOS, P123 block copolymer [poly(ethyleneglycol)–poly(propylene glycol)–poly(ethylene glycol), average molecu-

* Corresponding author. Fax: +91 20 25902633.
E-mail address: sb.halligudi@ncl.res.in (S.B. Halligudi).

0021-9517/$ – see front matter © 2008 Elsevier Inc. All rights reserved.
doi:10.1016/j.jcat.2008.05.015

lar mass 5800], and all of the sulfides were purchased from Aldrich Chemicals and used as received. The 70% aq. TBHP was procured from Acros Organics. All of the solvents procured from Merck (AR grade), India were distilled and dried before use. Titanium silicates (TS-1 and TS-2) were collected from the Catalysis Pilot Plant (CPP), National Chemical Laboratory, Pune (India).

2.2. Catalyst preparation

Hexagonally ordered mesoporous WO_x/SBA-15 nanocomposite materials were synthesized using tetraethylorthosilicate (TEOS) as the silica source and poly(ethylene oxide)-*block*-poly(propylene oxide)-*block*-poly(ethylene oxide) triblock copolymer (Aldrich, MW avg. 5800, $EO_{20}PO_{70}EO_{20}$, P123) as a structure-directing agent. In a typical synthesis, 4.0 g of P123 block copolymer was dissolved under stirring in a solution of 30.0 g of water and the required amounts (20, 10, 5, or 2.5 mL) of aqueous sodium tungstate solution ($NaWO_4{\cdot}2H_2O$, 0.5 M) were simultaneously added into the mixture under vigorous stirring. After 1 h, 120.0 g of HCl (2 M) and 9.1 g of TEOS were added under stirring at 40 °C. After 24 h of constant stirring, the gel composition was kept at 100 °C under static conditions for 48 h. After being cooled to room temperature, the solid product was recovered by filtering, washing, drying, and calcining at 550 °C. The nanocomposite samples were designated WO_x/SBA-15(v), where v denotes the volume of sodium tungstate solution [37].

2.3. Catalyst characterization

Tungsten content of the catalyst was determined by energy-dispersive X-ray analysis (EDAX) using Microanalysis Phoenix system. Nitrogen adsorption and desorption isotherms were measured at −196 °C with a Quantachrome Autosorb 1 sorption analyzer. The samples were outgassed for 3 h at 250 °C under vacuum in the degas port of the adsorption analyzer. The specific surface area was calculated using the BET model. The pore size distributions were obtained from the adsorption branch of the nitrogen isotherms by the Barrett–Joyner–Halenda method. The morphology and elemental mapping of the materials were analyzed using a Hitachi S-4800 field emission scanning electron microscope (HR-FESEM) with EDAX using an accelerating voltage of 10 kV. The X-ray diffraction (XRD) patterns of the samples were collected on a Philips X'Pert Pro 3040/60 diffractometer using Cu$K\alpha$ radiation ($\lambda = 1.5418$ Å), iron as the filter, and X'celerator as the detector. The high-resolution transmission electron microscopy (HRTEM) images and the elemental mapping were analyzed using a JEOL model 1200 microscope. The preparation of samples for HRTEM analysis involved sonication in isopropanol for 30 min, followed by deposition on a copper grid. The accelerating voltage of the electron beam was 120 kV. X-ray photoelectron spectroscopy (XPS) measurements were performed on a VG Microtech Multilab ESCA 3000 spectrometer with a nonmonochromatized Mg$K\alpha$ X-ray source. The resolution of the spectrometer was set at 0.8 eV with Mg$K\alpha$ radiation energy of 50 eV. The binding energy correction was performed using the C1s peak of carbon at 284.9 eV as a reference. Shimadzu FTIR-8201PC in DRS mode was used to obtain FTIR spectra of solid samples with a measurement range of 1400–700 cm^{-1}. The NMR spectrum of the catalyst was recorded using a Bruker DSX-300 spectrometer. Diffuse reflectance UV–visible (DRUV–vis) spectra of catalyst samples were obtained using a Shimadzu UV-2101 PC spectrometer equipped with a diffuse–reflectance attachment, with $BaSO_4$ as the reference. The reducibility of the calcined copper catalysts was measured by the TPR method using a Micromeritics AutoChem 2910 instrument. Raman spectra of the catalyst were recorded on powder samples at room temperature with a Bruker IFS 66 spectrometer connected to a Raman module FRA 106. The AFM images were obtained on a Digital Instruments Nanoscope IIIa SPM by tapping mode AFM.

2.4. Typical procedure for oxidation sulfides to sulfoxides

The liquid-phase catalytic oxidation of sulfides was conducted under atmospheric pressure at room temperature in a 50-mL reaction vessel equipped with a magnetic stirrer. In a typical experiment, substrate 2 mmol of substrate was oxidized using 3 eq. of 70% TBHP and 0.05 g of catalyst in CH_3OH:CH_2Cl_2 (1:1) (10 mL) at room temperature. The progress of the reaction was monitored by TLC and gas chromatography (GC) with a Shimadzu 14B gas chromatograph equipped with a capillary column (cross-linked 5% diphenyl–95% dimethylpolysiloxane capillary column, 30 m × 0.53 × 1.5 μm film thickness) and a flame ionization detector. After the reaction was complete, the reaction mixture was filtered off, and the catalyst was washed with dichloromethane (25–30 mL). The excess solvent was removed under reduced pressure to give the corresponding pure sulfoxide (Table 1). In most cases, the products were analyzed without no chromatographic purification by GC (Shimadzu 14B) and GC-mass spectroscopy (GC-MS) (Shimadzu (GC-17A & QP-5000) with identical columns. All known reaction products gave satisfactory GC mass and GCIR (Perkin–Elmer system 2000) spectra compared with those obtained from authentic samples. For di-*p*-tolylsulfoxides and *p*-nitrophenylmethylsulfoxides, after the usual workup, the crude sulfoxides were chromatographed on silica gel using a solvent mixture of hexane/ethyl acetate (10:1) as the eluent to afford the corresponding pure product confirmed by ^{1}H- and ^{13}C-NMR ($CDCl_3$, 200 MHz).

The resulting mixture was filtered to remove the catalyst, and the solvent was removed under reduced pressure. It was then dried in vacuum and purified by column chromatography on silica gel (60–120 mesh) as the stationary phase (petroleum ether/ethyl acetate, 50/50). Yield: 99%. Methylphenylsulfoxide: colorless liquid

^{1}H NMR ($CDCl_3$, 200 MHz): $\delta = 7.47$–7.53 (m, 3H), 7.60–7.65 (m, 2H), 2.69 (s, 3H). ^{13}C NMR ($CDCl_3$, 200 MHz): $\delta = 131.1$ (C), 129.3 (CH), 128 (CH), 127.3 (CH), 125.3 (CH), 123.5 (CH), 44 (CH_3). GCMS: m/z 140($M^{+\cdot}$), 125, 112, 97, 91, 77, 65, 51.

3. Results and discussion

3.1. Catalyst characterization

The wide-angle and low-angle XRD patterns of the WO_x/SBA-15 nanocomposite with different loading of WO_x are shown in Figs. 1A and 1B, respectively. All diffraction peaks could be indexed to monoclinic WO_3, which are in good agreement with those of bulk monoclinic crystal (JCPDS card no. 83-0951). The low-angle XRD measurements show that WO_x/SBA-15 materials exhibited three peaks at a 2θ in the range of 0.5–5°, which can be indexed to (100), (110), and (200) reflections of the hexagonal *p6mm* space group. The observation is in good agreement with the XRD pattern of pure hexagonally ordered SBA-15 material reported in the literature [38–40], indicating that the WO_x/SBA-15 materials have a well-ordered two-dimensional mesoporous structure with a hexagonal porous network. Fig. 1B clearly displays the peaks at higher angles, showing that the intensities of the peaks increased with increasing WO_x loading, confirming the presence of WO_x nanoclusters in the mesochannels of SBA-15. The size of the WO_x crystallites in the SBA-15 porous matrix was calculated to be 2–5 nm using Scherrer's equation. The nitrogen adsorption–desorption isotherms of SBA-15 and WO_x/SBA-15 nanocomposite were found to be type IV isotherms and a exhibit sharp increases in the amounts of nitrogen adsorbed at a relative pressure (P/P_0) of 0.6–0.9, typical features of curves of mesoporous structures,

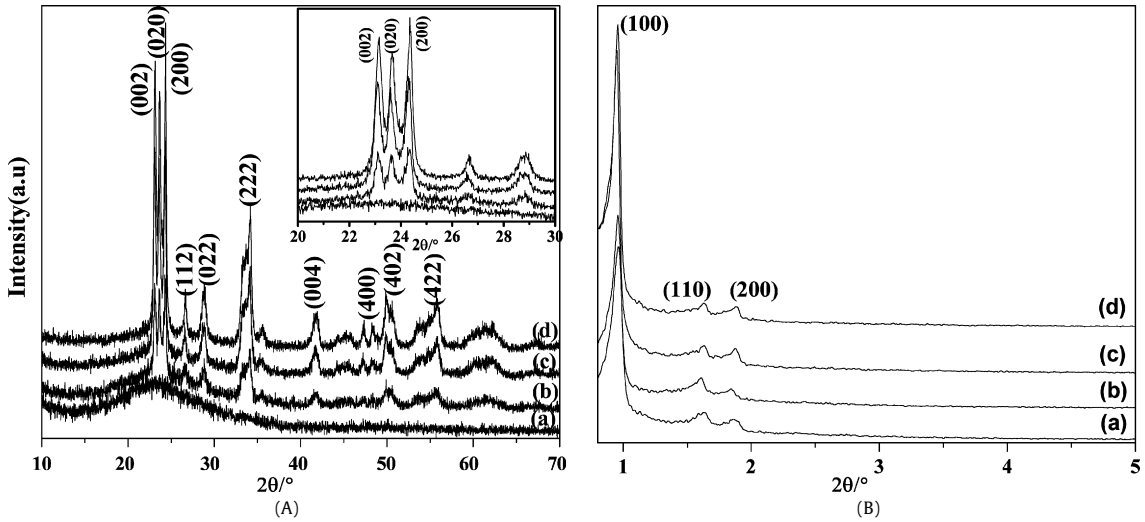

Fig. 1. (A) Wide and (B) low angle XRD patterns of WO_x/SBA-15 with different concentration of WO_x: (a) WO_x/SBA-15(2.5), (b) WO_x/SBA-15(5), (c) WO_x/SBA-15(10), (d) WO_x/SBA-15(20).

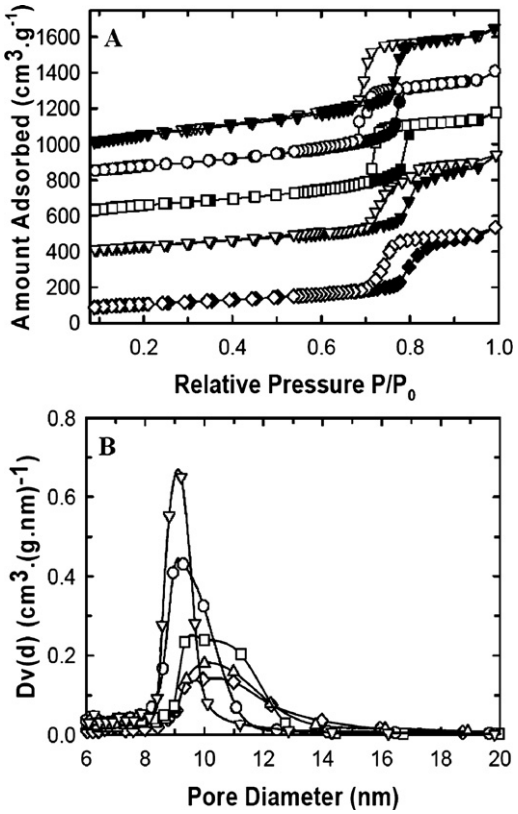

Fig. 2. (A) Nitrogen adsorption–desorption isotherms and (B) BJH adsorption pore size distributions of SBA-15 and WO_x/SBA-15: (△) SBA-15, (○) WO_x/SBA-15(2.5), (□) WO_x/SBA-15(5), (△) WO_x/SBA-15(10), and (◇) WO_x/SBA-15(20).

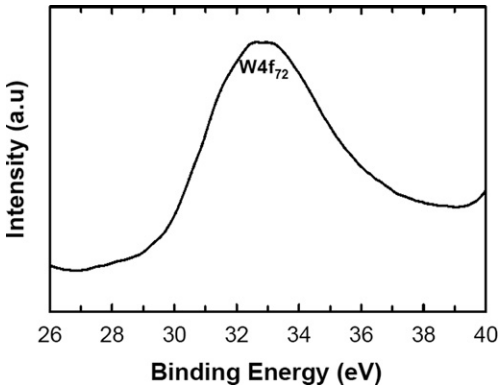

Fig. 3. XPS spectra of W4f of WO_x/SBA-15(20).

which were maintained in the WO_x/SBA-15 (Fig. 2) [41,42]. The amount of nitrogen adsorbed decreased with increasing loading of WO_x nanoclusters. Surface areas and pore volumes were lower for the WO_x/SBA-15 samples compared with the SBA-15 sample (Table 1). Interestingly, the WO_x/SBA-15 materials had larger pore diameters than pure SBA-15. The catalysts were characterized by XPS (Fig. 3), elemental mapping (Fig. 4), and EDAX to evaluate their elemental composition and purity. No peak of any metallic tungstate was observed in the XPS spectra of the as-prepared WO_x nanoclusters, indicating high purity of the material (Fig. 3). The broadening of the XPS peak could be due to the presence of tungsten species in various oxidation states. EDAX analysis of the material (Table 1) demonstrated the presence of W, Si, and O peaks.

HRTEM images of WO_x/SBA-15(20) nanocomposite (Fig. 5) show that the materials retained the hexagonally ordered porous structure even after the formation of WO_x nanoclusters in the

Table 1
Physicochemical properties of catalyst systems

No	Materials	Surface area ($m^2\,g^{-1}$)	Pore		EDAX analysis (%)					
			Volume ($cm^3\,g^{-1}$)	Diameter (nm)	W		Si		O	
					Wt	At. wt	Wt	At. wt	Wt	At. wt
1	SBA-15	910	1.25	9.2	0	0	38.1	26.0	61.9	74.0
2	WO_x/SBA-15(2.5)	632	1.02	9.3	2.5	0.3	40.0	28.3	57.5	71.4
3	WO_x/SBA-15(5)	562	0.98	10.0	8.1	0.9	34.7	25.5	57.2	73.6
4	WO_x/SBA-15(10)	464	0.88	10.0	20.5	2.6	30.3	25.3	49.2	72.1
5	WO_x/SBA-15(20)	321	0.69	10.0	36.9	5.8	26.6	27.6	36.5	66.6

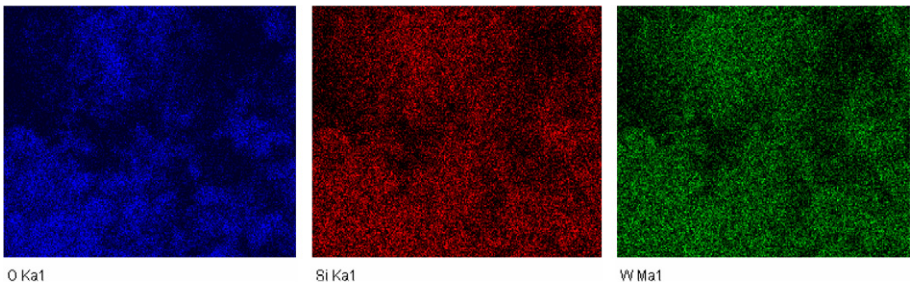

Fig. 4. Elemental mapping of WO_x/SBA-15(20).

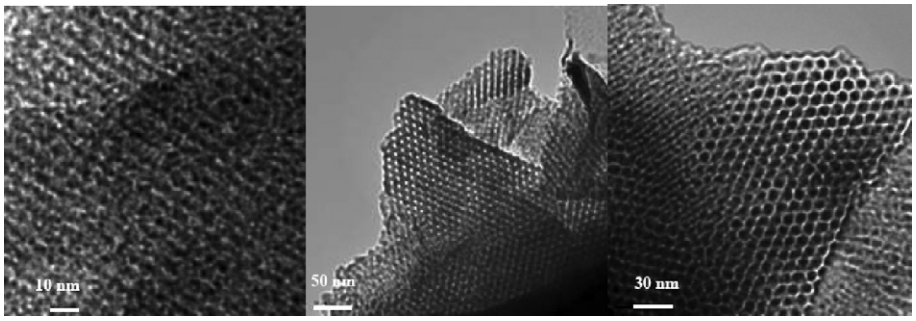

Fig. 5. HRTEM pictures of WO_x/SBA-15(20).

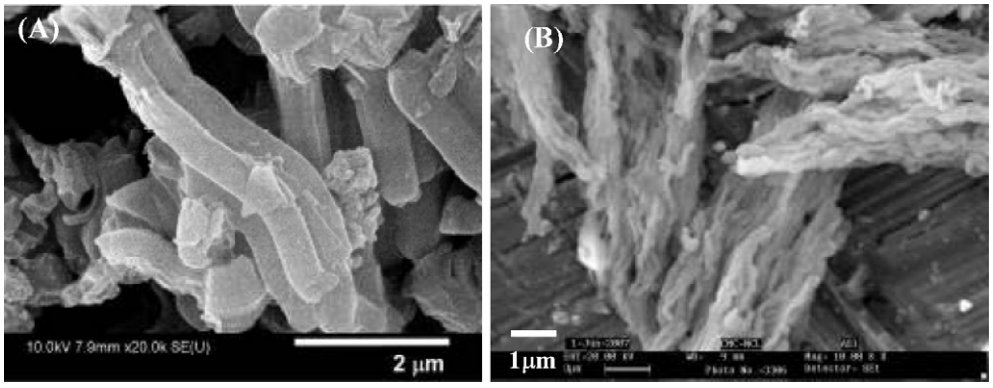

Fig. 6. HRSEM images of (a) SBA-15 and (b) WO_x/SBA-15(20).

mesochannels. But the WO_x nanoclusters are not visible in the HRTEM images, confirming that the WO_x nanoclusters were not deposited on the external surface but instead were present inside the mesochannels of SBA-15 [43]. The SEM images show that the morphology of WO_x/SBA-15(20) nanocomposite remained the same as that of the parent SBA-15 (Fig. 6). The AFM image of WO_x/SBA-15(20) clearly shows that the well-organized mesostructure was maintained on calcination, along with elimination of the organic template from the pore voids. On calcination, the template was eliminated, accompanied by the crystallization of WO_x, which decreased the long-range order and resulted in marginal collapse of mesopores (Fig. 7).

MAS NMR is a very attractive technique for characterizing surface protons in high-surface area materials. Fig. 8 shows ^{1}H NMR–MAS spectra of the WO_x/SBA samples. Fig. 8a shows the spectra for "as-synthesized" WO_x/SBA before and after calcination in air at 773 K. The "as- synthesized" NMR spectrum of WO_x/SBA exhibits two ^{1}H NMR lines centered at 2.5 and −0.56 ppm. The line at 2.5 ppm (Fig. 8a) is assigned to protons in H_2O and Si–OH interacting with one another through hydrogen bonding, with the latter (−0.56 ppm) reflecting the presence of isolated silanols (Si–OH). The line at 2.8 ppm seen in calcined sample WO_x/SBA-15 is

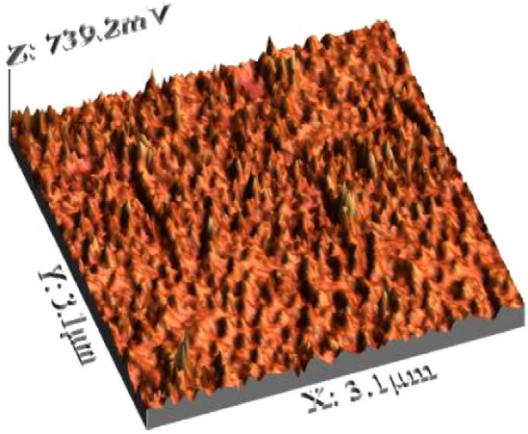

Fig. 7. AFM image of WO_x/SBA-15(20).

due to hydrogen-bonded hydroxyl groups and/or physisorbed water. Fig. 8b shows the ^{1}H NMR–MAS spectra of the WO_x/SBA-15 nanocomposite samples calcined at 773 K. The sharp line seen at 2.8 ppm is due to hydrogen-bonded hydroxyl groups and/or physi-

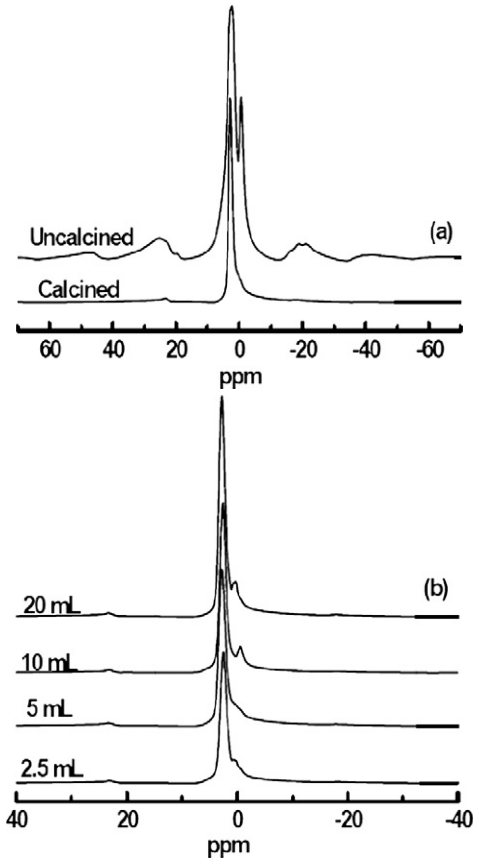

Fig. 8. (a) CP-MAS NMR profile of calcined and uncalcined WO_x/SBA-15(20), (b) CP-MAS NMR profile of WO_x/SBA-15 with different concentration of WO_x.

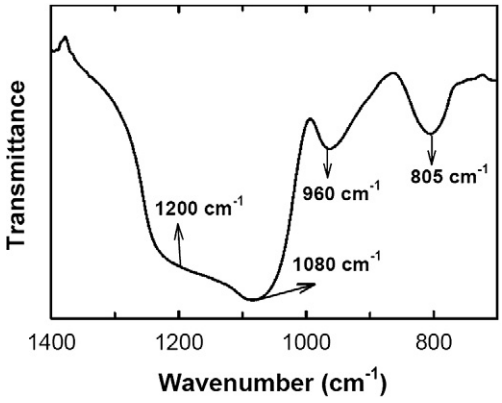

Fig. 9. FTIR spectrum of WO_x/SBA-15(20).

sorbed water, whereas the small hump seen at 0.28 ppm for the WO_x/SBA-15 samples could be due to water molecules hydrogen-bonded to W–OH protons [44,45].

FTIR spectroscopy in the skeletal region at 400–700 cm^{-1} was used to follow the variation of the structure of WO_x/SBA-15(20). Typical bands due to siliceous material Si–O–Si were observed for both the parent and the WO_x/SBA-15(20) (Fig. 9): a main band at 1080 cm^{-1}, with a shoulder at 1200 cm^{-1} due to asymmetric Si–O–Si stretching modes and symmetric stretch at 805 cm^{-1}, and an additional band at ca. 960 cm^{-1}, which is widely used to characterize the presence of transition metal atoms near the silica framework as the stretching Si–O vibration mode perturbed by the neighboring metal ions. Thus, the presence of such an IR band due to perturbed silica vibrations can be attributed to the formation of WO_x nanoclusters in SBA-15.

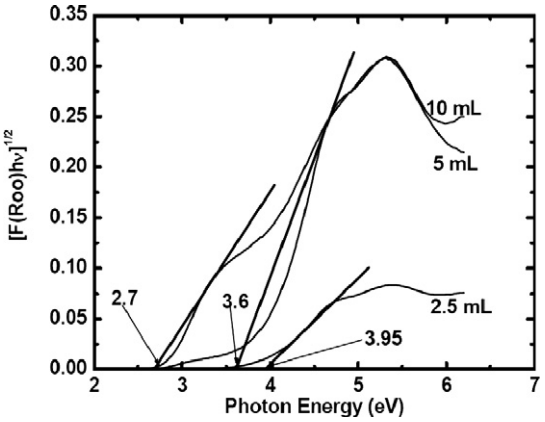

Fig. 10. UV–vis DRS spectra for three WO_x/SBA-15 samples with different tungsten loadings. $[F(R\infty)h\nu]$ represents the Kubelka–Munk function multiplied by the photon energy.

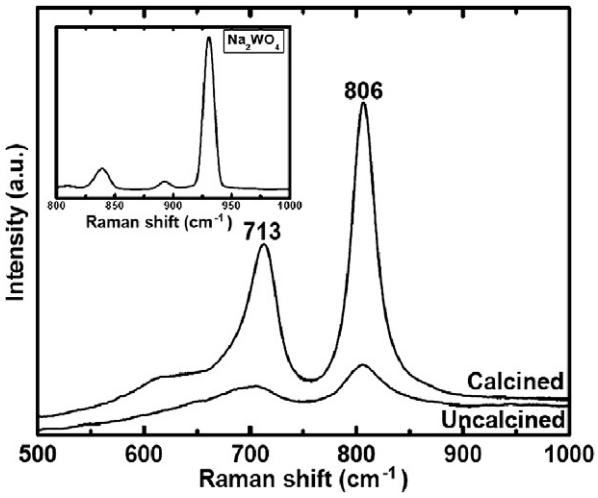

Fig. 11. Raman spectra of calcined and uncalcined samples of WO_x/SBA-15(20). Inset: Raman spectra of $Na_2WO_4{\cdot}2H_2O$.

The optical absorption edge energies of WO_x/SBA-15 nanocomposite samples were obtained from the DRUV–vis absorption spectra. The optical absorption edge energy is defined as the minimum photon energy required to excite an electron from the highest occupied molecular orbital (HOMO; at the top of the valence band in semiconductor domains) to the lowest unoccupied molecular orbital (LUMO; at the bottom of the conduction band). There are two basic types of electronic transitions: direct and indirect. Direct transitions require only that photons excite electrons, whereas indirect transitions require concerted vibrations and energy from the crystal lattice (phonons). For dispersed WO_x domains, Barton et al. used the square root of the Kubelka–Munk function multiplied by the photon energy, which allows the edge energy to be obtained by extrapolation to zero absorbance for amorphous semiconductors. The values thus obtained carry information about the average domain size of the oxide nanoparticles, although the values depend on local symmetry and support electronegativity. Fig. 10 shows DRUV–vis spectra for the WO_x/SBA-15 samples. All of the WO_x/SBA-15 catalysts exhibited main absorption features at energies ranging from 3.5 to 2.6 eV due to ligand-to-metal charge transfers in tungsten species on the SiO_2 surface, as reported by Herrera et al. [8] and Barton et al. [44].

We performed Raman experiments to determine in which synthesis step (WO_x/SBA-15) were the WO_x nanoclusters formed. Raman bands corresponding to crystalline WO_3 (Fig. 11) appeared at 806 and 713 cm^{-1}; these bands corresponded to W–O stretching

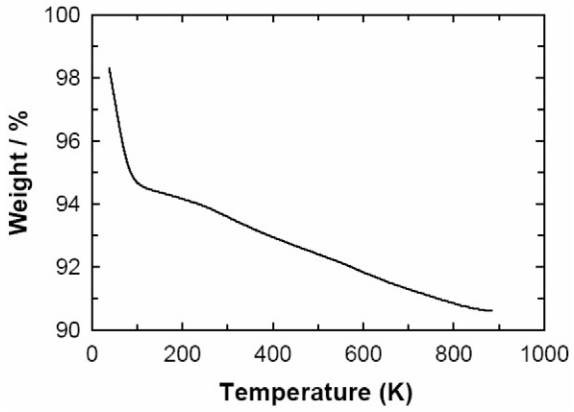

Fig. 12. TGA plot of WO_x/SBA-15(20).

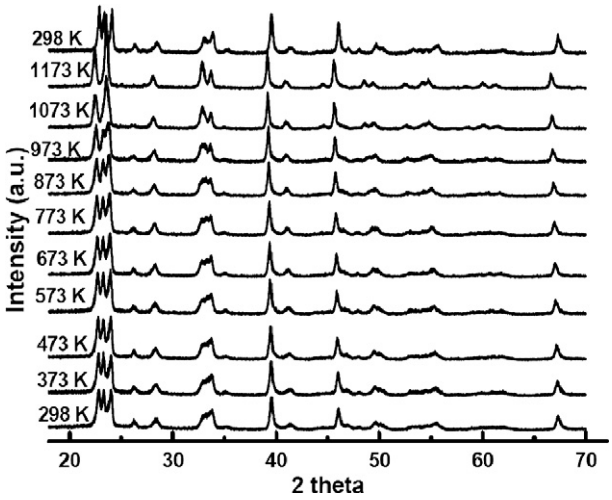

Fig. 13. X-ray diffraction patterns of WO_x/SBA-15(20). The diffractograms were obtained in situ during thermal treatment at the indicated temperatures.

and bending modes, respectively, in both calcined and uncalcined materials [43]. The Raman bands of uncalcined materials are of comparatively lower intensity than those of the calcined materials. However, the Raman bands of the cubic Na_2WO_4 phase were observed at 932 and 840 cm^{-1}, corresponding to internal vibrations of WO_4 (Fig. 11, inset). This indicates that the formation of WO_x nanoclusters started in the aging step of their synthesis. The weight loss detected in the thermogravimetric analysis (TGA) of the calcined WO_x/SBA-15(20) sample below 373 K was related to desorbed water (Fig. 12).

Fig. 13 shows temperature-resolved PXRD patterns of the WO_x/SBA-15(20) sample collected at 298–1173 K at 100-K intervals and again at room temperature. Clearly, the WO_x/SBA-15(20) material exhibited a monoclinic phase in the temperature range studied, in agreement with literature reports. The data quality of the scan was comparatively good, due to the use of the X'celerator detector, which uses real-time multiple-strip technology to enhance both the resolution and intensity of the reflections. The multiple plots of the powder patterns measured in static air indicate the stability of the monoclinic phase of WO_x at temperatures as high as 1123 K. Above 1023 K, the expected anatase-to-rutile phase transformation was observed. The powder pattern of the sample obtained after cooling to room temperature was similar to that seen at high temperature (298 K), indicating a reversible anatase-to-rutile phase transformation.

Temperature-programmed reduction (TPR) with hydrogen is widely used to characterize reducible solids and catalysts. In TPR,

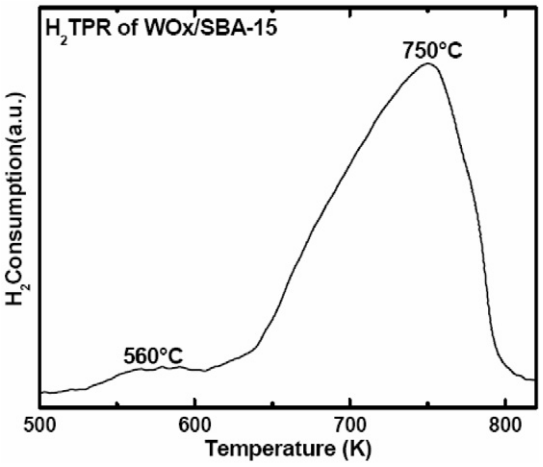

Fig. 14. Temperature programmed reduction profile of catalyst: WO_x/SBA-15(20).

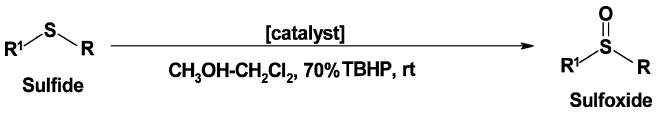

Scheme 1. Oxidation of sulfide to sulfoxide.

Table 2
WO_x/SBA-15(20) catalyzed oxidation of sulfides to sulfoxides with 70% aq. TBHP[a]

Entry	R	R^1	Yield (%)[b]
1	Me	Ph	99
	1st		97[c]
	2nd		95[c]
	3rd		91[c]
	4th		90[c]
2	Et	Ph	99
3	*i*-Pr	Ph	99
4	$-CH_2-C_6H_5$	Ph	95
5	$-CH_2-p$-Tol	4-Me–C_6H_4	99
6	Me	4-MeO–C_6H_4	99
7	$-CH_2-CH_2CH_2$	Ph	92[d]
8	Ph	Ph	95
9	Me	2-Cl–C_6H_4	68
10	Me	4-Cl–C_6H_4	65
11	Me	4-Br–C_6H_4	68
12	Me	4-NO_2–C_6H_4	49
13	Et	Et	99
14	$-CH_2-C_6H_5$	$-CH_2-C_6H_5$	92

[a] Reaction conditions: substrate (2 mmol) using 70% TBHP (3 equiv.) and catalyst (0.05 g) in CH_3OH:CH_2Cl_2 (1:1) (10 mL) at room temperature.
[b] Isolated yields. GC conversion unless otherwise stated.
[c] Recycling experiment.
[d] No epoxidation product was detected.

a reducible catalyst or catalyst precursor is exposed to a flow of a reducing gas mixture (typically a few vol% of hydrogen in an inert gas) as the temperature is increased linearly. According to previous reports [45], pure WO_3 exhibits three reduction peaks: a shoulder at 560 °C ($WO_3 \rightarrow W_{20}O_{58}$), a sharp peak at 750 °C ($W_{20}O_{58} \rightarrow WO_2$) and a peak at higher temperature ($WO_2 \rightarrow W$). Pure SiO_2 exhibited no detectable TPR peak at temperature below 1000 °C; thus, the reduction peaks observed (Fig. 14) can be attributed to the reduction of WO_x only.

3.2. Catalytic oxidation of sulfides

To evaluate catalytic activity, we selected the oxidation of methylphenylsulfide using 70% TBHP as a model reaction at room temperature (Scheme 1). The catalyst gave excellent yields of corresponding sulfoxide in 10 h (Table 2, entry 1), with no overox-

Table 3
Comparison of different catalysts in oxidation of ethylphenylsulfide[a]

Entry	Catalyst	Conversion (mol%)	Selectivity of sulfoxide (mol%)
1	WO_x/SBA-15(20)	100	99
2	TS-1	10	100
3	TS-2	90	80

[a] Reaction conditions: substrate (2 mmol) using 70% TBHP (3 equiv.) and catalyst (0.05 g) in CH_3OH:CH_2Cl_2 (1:1) (10 mL) at room temperature.

idation of sulfides to sulfones. The efficiency of TBHP for the aforementioned reaction was evaluated based on the amount of oxidative products produced from methylphenylsulfide divided by the amount of TBHP consumed. We found 99% conversion of TBHP, demonstrating the 100% efficiency of TBHP. In the absence of the catalyst, no significant oxidation was observed under similar reaction conditions.

In a similar way, various types of structurally diverged aryl alkyl sulfides underwent smooth oxidation to selectively afford the corresponding sulfoxides in excellent yields (Table 2, entries 2–6). Another useful feature of the present protocol can be seen in the selective oxidation of allyl phenyl sulfide to corresponding sulfoxide; neither overoxidation to the sulfone nor epoxidation of the double bond and corresponding sulfoxide was obtained in good yields (Table 2, entry 7). Interestingly, under the present reaction conditions, even hindered diaryl sulfides furnished corresponding sulfoxides in excellent yields (Table 1, entry 8). The compounds that have an electron-withdrawing ring substituent, such as bromo or chloro, are less reactive (Table 2, entries 9–11). Also of note is the finding that the strong electron-withdrawing NO_2 group on the phenyl ring had little effect on the efficiency of synthesis (Table 2, entry 12). Interestingly, however, the corresponding sulfoxides formed under the protocol for the oxidation of dialkyl sulfides. We found that under the similar reaction conditions, diethyl sulfide was converted to diethyl sulfoxide in excellent yield (Table 2, entry 13), and dibenzyl sulfide furnished the corresponding sulfoxide in high yield (Table 2, entry 14). We studied catalyst stability and recyclability using standard procedures; the results clearly demonstrate the practical reusability of the reported catalyst system. We also studied the oxidation of methylphenylsulfide with 70% TBHP using TS-1 and TS-2 under similar reaction conditions. The results, presented in Table 3, show that TS-1 had negligible activity, whereas TS-2 had comparable activity to WO_x/SBA-15(20) but with lower sulfoxide selectivity [46,47]. Undoubtedly, our proposed catalyst system is very active in the oxidation of methylphenylsulfide to give sulfoxides selectively at room temperature.

3.3. Catalyst stability and recyclability

WO_x/SBA-15(20) was used to establish the stability of the catalyst in recycling experiments. XRD and EDAX experiments were performed to establish the stability of the catalyst system after recycling. Fig. 15 presents wide-angle and small-angle XRD patterns of the first, third, and seventh catalyst recyclings. The wide-angle XRD patterns are comparable with those obtained for the fresh catalyst (Fig. 1). The small-angle XRD patterns show a decrease in the intensities of the peaks, possibly due to a marginal loss of order in the material after recycling. But the presence of three well-resolved peaks in XRD patterns of the catalysts after the seventh recycling indicates the retention of a well-ordered WO_x/SBA-15(20) structure. The EDAX data (Table 4) also support the good structural integrity of the material after recycling.

We carried out two additional experiments to investigate the stability of WO_x/SBA-15(20) system toward a strong oxidant such as TBHP. To check the leaching of WO_x species from the catalytic system into the reaction medium, we treated a fresh WO_x/SBA-15(20) sample with a freshly prepared reaction mixture, and then carried out the reaction at room temperature for 24 h. The reaction mixture was then filtered to separate catalyst, and the filtrate was analyzed for the presence of tungsten. The catalyst separated as described earlier after the first recycling was treated in another fresh reaction mixture, and the filtrate was analyzed for tungsten. As before, this catalyst was recycled 7 times. ICP-AES analysis of all of the recycling experiments demonstrated the complete absence of tungsten in the reaction mixture.

The foregoing results confirm the stability of the WO_x/SBA-15 (20) system, with no leaching of active species WO_x seen even after the seventh recycling. These results demonstrate the practical reuse of the reported catalyst system under the reaction conditions used here.

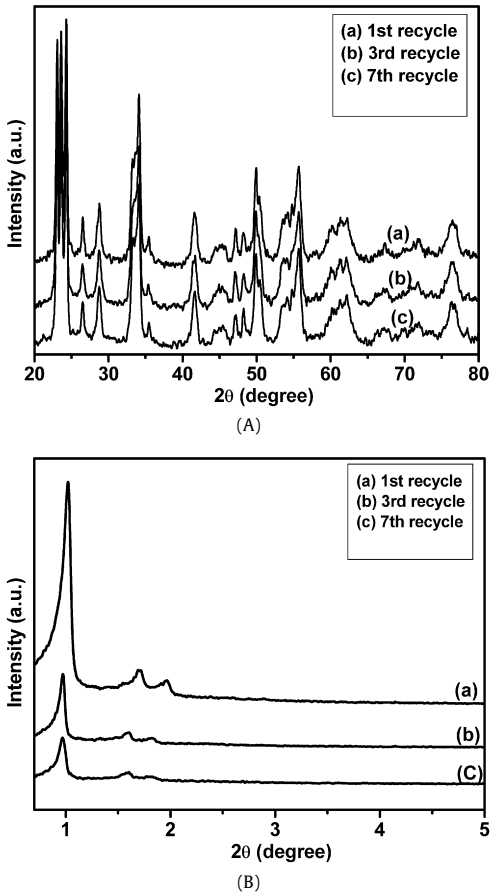

Fig. 15. (A) Wide and (B) low angle XRD patterns of recycled WO_x/SBA-15(20): (a) 1st recycle, (b) 3rd recycle, and (c) 7th recycle.

Table 4
EDAX analysis data of recycled catalyst WO_x/SBA-15(20)

Recycles	EDAX analysis (%)					
	W		Si		O	
	Wt	At. wt	Wt	At. wt	Wt	At. wt
1st	36.9	5.8	26.6	27.6	36.5	66.6
3rd	36.8	5.7	26.6	27.6	36.7	66.7
7th	36.8	5.7	26.5	27.5	36.8	66.8

4. Conclusion

We have successfully demonstrated that highly dispersed WO_x nanoclusters in the mesochannels of SBA-15 can be prepared by in situ hydrothermal method in a highly acidic medium. The catalyst exhibits high catalytic activity for the oxidation of sulfur com-

pounds due to the presence of highly dispersed tungsten oxide species in the SBA-15 mesochannels. The enhanced chemoselectivity at higher substrate conversions achieved over this catalyst are attributed to the unique large pore diameters and low surface acidity of WO_x/SBA-15, which enable the facile discharge of the desired products from the channels of the catalyst under ambient conditions. In addition, the catalyst is recyclable with no loss in activity. This strategy could be used for similar chemical transformations in an eco-friendly manner.

Acknowledgment

A.B. thanks CSIR New Delhi for the award of a research fellowship.

References

[1] M.D. Hughes, Y.-J. Xu, P. Jenkins, P. McMorn, P. Landon, D.I. Enache, A.F. Carley, G.A. Attard, G.J. Hutchings, F. King, E.H. Stitt, P. Johnston, K. Griffin, C.J. Kiely, Nature 437 (2005) 1132.
[2] B. Vishwanathan, S. Sivasanker, A.V. Ramaswamy (Eds.), Catalysis: Principles and Application, Narosa Publishing House, New Delhi, 2007, p. 147.
[3] D.J. Cole-Hamilton, Science 299 (2003) 1702.
[4] X.-L. Yang, W.-L. Dai, H. Chen, Y. Cao, H. Li, H. He, K. Fan, J. Catal. 229 (2005) 259.
[5] J. Jarupatrakorn, M.P. Coles, T.D. Tilley, Chem. Mater. 17 (2005) 1818.
[6] Z. Zhang, J. Suo, X. Zhang, S. Li, Appl. Catal. A Gen. 179 (1999) 11.
[7] E. Briot, J.-Y. Piquemal, M. Vennat, J.-M. Bregeault, G. Chottard, J.-M. Manoli, J. Mater. Chem. 10 (2000) 953.
[8] J.E. Herrera, J.H. Kwak, J.Z. Hua, Y. Wang, C.H.F. Peden, J. Macht, E. Iglesia, J. Catal. 239 (2006) 200.
[9] R.A. Sheldon, J.K. Kochi (Eds.), Metal Catalyzed Oxidation of Organic Compounds, Academic Press, New York, 1981, p. 5.
[10] J.-E. Bäckvall (Ed.), Modern Oxidation Methods, Wiley–VCH, Weinheim, 2004, p. 4.
[11] G. Soladie, Synthesis 3 (1981) 185.
[12] M.C. Carreno, Chem. Rev. 95 (1995) 1917.
[13] J. Fuhrhop, G. Penzlin (Eds.), Organic Synthesis, Concepts, Methods, Starting Materials, second ed., Wiley–VCH, Weinheim, 1994, p. 26.
[14] E. Block (Ed.), Reaction of Organosulfur Compounds, Academic Press, New York, 1978, p. 15.
[15] C.G. Venier, T.G. Squires, Y.Y. Chen, G.P. Hussmann, J.C. Shei, B.F. Smith, J. Org. Chem. 47 (1982) 3773.
[16] R.W. Murray, R. Jeyaraman, J. Org. Chem. 50 (1985) 2847.
[17] S.W. Kaldor, M. Hammond, Tetrahedron Lett. 32 (1991) 5043.
[18] W. Adam, L. Hadjiarapoglou, Tetrahedron Lett. 33 (1992) 469.
[19] G.W. Breton, J.D. Fields, P.J. Kropp, Tetrahedron Lett. 36 (1995) 3825.
[20] D.H.R. Barton, W. Li, J.A. Smith, Tetrahedron Lett. 39 (1998) 7055.
[21] M. Hirano, S. Yakabe, J.H. Clark, T. Morimoto, J. Chem. Soc. Perkin Trans. 1 (1996) 2693.
[22] R.A. Sheldon, M. Wallau, I.W.C.E. Arends, U. Schuchardt, Acc. Chem. Res. 31 (1998) 485.
[23] A. Corma, H. Garcia, Chem. Rev. 103 (2003) 4307.
[24] C. Venturello, R. D'Aloisio, J.C.J. Bart, M. Ricci, J. Mol. Catal. 32 (1985) 107.
[25] W.A. Herrmann, J. Fridgen, G.M. Lobmaier, M. Spiegler, New. J. Chem. 23 (1999) 5.
[26] D. Sloboda-Rozner, P.L. Alsters, R. Neumann, J. Am. Chem. Soc. 125 (2003) 5280.
[27] K. Sato, M. Aoki, R. Noyori, Science 281 (1998) 1646.
[28] B.F. Sels, D.E. De Vos, P.A. Jacobs, J. Am. Chem. Soc. 123 (2001) 8350.
[29] F.M. Collins, A.R. Lucy, C. Sharp, J. Mol. Catal. A Chem. 117 (1997) 397.
[30] C. Venturello, R. D'Aloisio, J. Org. Chem. 53 (1988) 1553.
[31] K. Kamata, K. Yonehara, Y. Sumida, K. Yamaguchi, S. Hikichi, N. Mizuno, Science 300 (2003) 964.
[32] M.V. Vasylyev, R. Neumann, J. Am. Chem. Soc. 126 (2004) 884.
[33] B. Karimi, M. Ghoreishi-Nezhad, J.H. Clark, Org. Lett. 7 (2005) 625.
[34] K. Yamaguchi, C. Yoshida, S. Uchida, N. Mizuno, J. Am. Chem. Soc. 127 (2005) 530.
[35] Y.M.A. Yamada, M. Ichinohe, H. Takahashi, S. Ikegami, Org. Lett. 3 (2001) 1837.
[36] X. Zuwei, Z. Ning, S. Yu, L. Kunlan, Science 292 (2001) 1139.
[37] A. Bordoloi, A. Vinu, S.B. Halligudi, Chem. Commun. (2007) 4806.
[38] D. Zhao, J. Feng, Q. Huo, N. Melosh, G.H. Fredrickson, B.F. Chmelka, G.D. Stucky, Science 279 (1998) 548.
[39] D. Zhao, Q. Huo, J. Feng, B.F. Chmelka, G.D. Stucky, J. Am. Chem. Soc. 120 (1998) 6024.
[40] H. Song, R.M. Rioux, J.D. Hoefelmeyer, R. Komor, K. Niesz, M. Grass, P. Yang, G.A. Somorjai, J. Am. Chem. Soc. 128 (2006) 3027.
[41] Y.J. Han, J.M. Kim, G.D. Stucky, Chem. Mater. 12 (2000) 2068.
[42] X.L. Yang, W.L. Dai, H. Chen, J.H. Xu, Y. Cao, H.X. Li, K.N. Fan, Appl. Catal. A 283 (2005) 1.
[43] P. Kustrowski, L. Chmielarz, R. Dziembaj, P. Cool, E.F. Vansant, J. Phys. Chem. B 109 (2005) 11552.
[44] D.G. Barton, M. Shtein, R.D. Wilson, S.L. Soled, E. Iglesia, J. Phys. Chem. B 103 (1999) 630.
[45] M.G. Falco, S.A. Canavese, N.S. Fıgoli, Catal. Today 107 (2005) 778.
[46] R.S. Reddy, J.S. Reddy, R. Kumar, P. Kumar, J. Chem. Soc. Chem. Commun. (1992) 84.
[47] S.V.N. Raju, T.T. Upadhya, S. Ponrathnam, T. Danie, A. Sudalai, Chem. Commun. (1996) 1969.